Directional quasi-phase matching AlGaAs waveguide microresonators for efficient generation of quadratic frequency combs

Maria Parisi[a], Iolanda Ricciardi[a], Simona Mosca[a], Natália Morais[b], Tobias Hansson[c], Stefan Wabnitz[d,a], Giuseppe Leo[b] and Maurizio De Rosa[a]

[a]CNR-INO, Istituto Nazionale di Ottica, Via Campi Flegrei 34, 80078 Pozzuoli (NA), Italy;
[b]Laboratoire Matériaux et Phénomènes Quantiques, Université Paris Diderot & CNRS, Sorbonne Paris Cité, 10 rue Domon et Duquet, 75205 Paris cedex 13, France;
[c]INRS-EMT, 1650 Blvd. Lionel-Boulet, Varennes, Québec J3X 1S2, Canada;
[d]Dipartimento di Ingegneria dell'Informazione, Università di Brescia, Via Branze 38, 25123 Brescia, Italy

ABSTRACT

Optical frequency combs currently represent enabling components in a wide number of fast-growing research fields, from frequency metrology to precision spectroscopy, from synchronization of telecommunication systems to environmental and biomedical spectrometry. As recently demonstrated, quadratic nonlinear media are a promising platform for optical frequency combs generation, through the onset of an internally pumped optical parametric oscillator in cavity enhanced second-harmonic generation systems. We present here a proposal for quadratic frequency comb generation in AlGaAs waveguide resonators. Based on the crystal symmetry properties of the AlGaAs material, quasi-phase matching can be realized in curved geometries (directional quasi-phase matching), thus ensuring efficient optical frequency conversion. We propose a novel design of AlGaAs waveguide resonators with strongly reduced total losses, compatible with long-path, high-quality resonators. By means of a numerical study, we predict efficient frequency comb generation with threshold powers in the microwatt range, paving the way for the full integration of frequency comb synthesizers in photonic circuits.

Keywords: Microresonators, AlGaAs, Optical frequency combs, Nonlinear optics.

1. INTRODUCTION

Waveguide microresonators provide small volume confinement and resonant field enhancement that greatly improves the efficiency of nonlinear processes. Resonant nonlinear devices also permit to implement new light sources such as, for instance, Kerr optical frequency combs (OFCs), exploiting third-order nonlinear interactions.[1] Recently, OFC generation was also demonstrated and theoretically modeled in nonlinear cavities with bulk second-order media.[?,2,5] Based on the lowest-order nonlinear interaction, $\chi^{(2)}$, OFCs can be inherently more efficient than Kerr combs and are capable of ultra-broadband multi-octave emission.[6] In a nonlinear cavity that is phase matched for second-harmonic generation (SHG), the generated harmonic power can reach the threshold for parametric oscillation leading to an internally pumped optical parametric oscillator (IP-OPO), which triggers a cascade of secondary three-wave processes, eventually forming frequency combs around the fundamental frequency (FF) and its second harmonic (SH). A lower threshold, thus a higher efficiency, can be achieved by exploiting materials with a strong quadratic coupling constant and maintaining a phase matching relation between the interacting fields over a sufficiently long interaction path.

GaAs and its AlGaAs alloy are one of most promising material platforms for integrated photonic circuits operating in the infrared range, with a transparency window extending from 0.7 to 17 μm. This platform is extensively used in numerous devices like waveguides, microresonators, lasers, amplifiers, and modulators.[7] Moreover, aluminum gallium arsenide (AlGaAs) has a strong quadratic nonlinear response, which makes it ideal for

Further author information: (Send correspondence to Maurizio De Rosa)
Maurizio De Rosa: E-mail: maurizio.derosa@ino.it, Telephone: +39 081 8675413

Quantum Sensing and Nano Electronics and Photonics XIV, edited by Manijeh Razeghi,
Proc. of SPIE Vol. 10111, 1011120 · © 2017 SPIE · CCC code: 0277-786X/17/$18
doi: 10.1117/12.2256290

the development of nonlinear photonic devices.[8,9] Although it lacks of natural birefringence, phase matching in AlGaAs can be realized in alternative different ways, such as form-birefringence phase matching, modal phase matching, domain-reversal quasi-phase matching, and domain disordered quasi-phase matching.[7] Interestingly, owing to the crystal symmetry of the AlGaAs structure, the effective nonlinear coupling depends on the direction of the interacting vector fields with respect to the crystal axes. This directional dependence has suggested a natural QPM scheme for second-harmonic generation in (Al)GaAs microdisks[10–13] and curved waveguides.[14] In this work, we propose a novel design for AlGaAs waveguide resonators, where a closed-loop sequence of arc- and S-shaped segments forms resonant configurations exploiting directional quasi-phase matching (DQPM). Geometric tailoring of the dispersive features, through a suitable device design, relaxes the constraint on waveguides curvature and allows to obtain internal losses compatible with long-path high-quality resonators. Supported by numerical simulations, we show the possibility to generate frequency combs, both at the FF and its SH, with pump power thresholds as low as a few μW and teeth separations in the range of 10-1000 GHz.

2. DIRECTIONAL QUASI-PHASE MATCHING

In every three-wave nonlinear generation process inside quadratic materials, because of chromatic dispersion, the interacting waves propagate with different phase velocities, thus accumulating a relative phase shift. This causes an energy flow that repeatedly goes back and forth amongst the fields as the beams propagate through the nonlinear medium. This is detrimental to the growth of the new generated frequencies and different methods can be adopted to achieve phase matching and optimize conversion efficiency. In birefringent materials, for example, phase matching can be achieved by properly choosing polarization, crystal cut, and crystal temperature, so that the birefringence compensates for dispersion. Alternatively, quasi-phase matching techniques compensate for the phase mismatch by regularly rephasing the interacting waves, e.g., by reversing the sign of the nonlinearity, as it occurs in periodically poled ferroelectric crystals, where the ferroelectric domains are permanently reversed.

The fulfillment of the phase matching condition is a crucial aspect in AlGaAs waveguides, where the lack of birefringence and ferroelectricity prevents the realization of the aforementioned schemes. Nevertheless, the crystal symmetry of the AlGaAs structure allows for the implementation of a natural quasi-phase matching scheme. Indeed, materials like AlGaAs belong to the $\bar{4}3m$ crystal symmetry of the zinc-blende structure for which, as shown in Fig. 1(a), a 90° rotation of the face-centered unit cell around a crystal axis is equivalent to a crystallographic inversion and, from the point of view of the nonlinear response, to an effective inversion of the sign of the nonlinear coupling. Actually, the only non-zero elements of the second order nonlinear tensor are $d_{14} = d_{25} = d_{36}$, which couple three interacting field components, each with a polarization along a different crystal axis. Thus, a TE-polarized electromagnetic pump field guided in a curved path laying in the x-y plane undergoes a change of the effective nonlinear coupling constant, depending on the field polarization direction (or angle) with respect to the crystal axes, Fig. 1(b). When we consider a uniform AlGaAs microdisk, as in Fig. 1(c), fields propagating around the z axis encounter four inversions of the nonlinear coupling per round trip. In order to phase match a specific nonlinear process, such as SHG in our case, the length of each arc (AB in Fig. 1(b)) must be equal to the corresponding coherence length $L_c = \pi/|\Delta k|$, where Δk is the wave-vector mismatch for SHG (see below for complete definitions).

The design of AlGaAs microdisk resonators actually has the following limitations: for a given pump frequency, the disk circumference C, i.e., the round trip interaction length, is univocally determined and limited to four coherence lengths, according to the phase matching condition. As a consequence, the resonator free spectral range, FSR$= c/n\,C$, with c the speed of light and n the refractive index, is fixed as well. For example, the directional quasi-phase matching condition for SHG with fundamental wavelengths in the near infrared implies disk radii ~ 2 μm, hence FSRs of several THz around the pump frequency.[15,16]

We propose to extend DQPM to more complex geometries in curve shaped waveguides, which can preserve phase matching over resonator lengths of up to several millimiters. These waveguides can be assembled according to a modular design, by combining a sequence of L_c-long, arc- and S-shaped segments in a loop with a total round trip length equal to an integer multiple of $2L_c$. For the sake of simplicity, we consider here circular arcs (A) of radius $2L_c/\pi$ and S-shaped segments (S) made by two circular arcs of radius L_c/π. For this particular choice, from simple geometric arguments, the spatial modulation of d_{14} can be derived as $\sigma_A(\zeta) = \pm|\sin(\pi\zeta/L_c)|$ and $\sigma_S(\zeta) = \pm|\sin(2\pi\zeta/L_c)|$, for A and S segments, respectively, as a function of the coordinate ζ denoting the

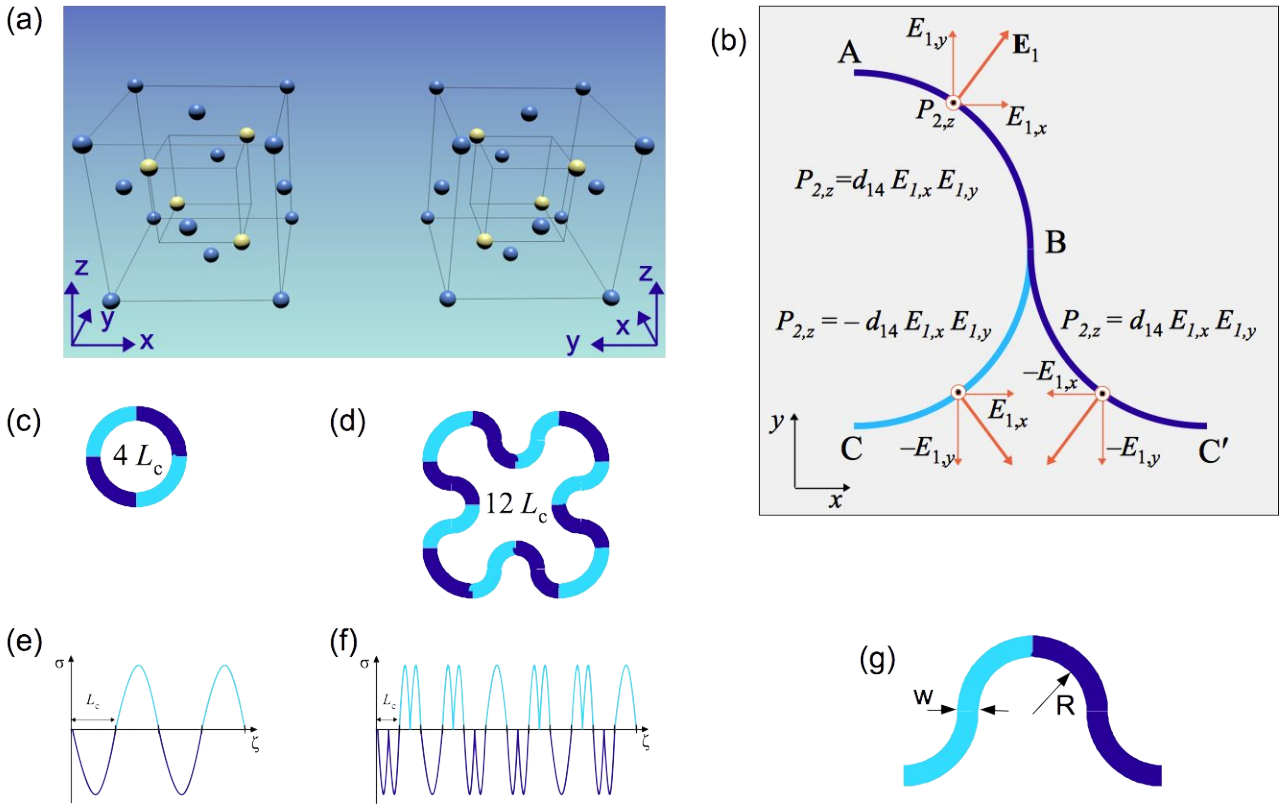

Figure 1. (a) Zinc blende structure of GaAs. A 90° rotation of the face-centered unit cell around the z-axis is equivalent to a crystallographic inversion. (b) The spatial modulation of the nonlinear coupling for a TE e.m. wave $\mathbf{E}_1$ propagating through a curved waveguide laying in the x-y crystal plane. (c) and (d) Examples of waveguide microresonator design for directional QPM: (c) a circular guide with a circumference four times the coherence length; (d) a 12 L_c-long resonant waveguide, made by arcs and S-shaped segments. (e) and (f) The associated normalized spatial modulation of the nonlinear coupling $\sigma(\zeta)$ for the structures of (c) and (d), respectively. (g) Geometrical parameters w and R of the simulated snake-shaped waveguide.

position along the waveguide path ($\zeta \in [0, L_c]$). The sign of σ_A depends on the orientation of the segment with respect to the crystal axes. A sequence of A- and S-segments will thus exhibit an effective nonlinear coupling defined by the corresponding sequence of σ_A's and σ_S's [Fig. 1(e) and (f)].

2.1 $Al_{0.18}Ga_{0.82}As$ waveguide microresonators

Hereafter, we focus our analysis on a specific suspended waveguide geometry[17] based on an air-surrounded $Al_{0.18}Ga_{0.82}As$ core, which grants for transparency at both FF and SH for a chosen fundamental wavelength around 1.55 μm, in view of the wide range of applications in the telecom band and optoelectronic industry.

For such resonators, a crucial issue is to keep the internal losses as low as possible, in order to efficiently recirculate the light over many round trips. Neglecting the technologically limited scattering losses, due to the roughness of the waveguide surfaces, curved waveguides are inherently affected by bending losses, which essentially grow inversely with the radius of curvature of the guide. Moreover, the sudden change of curvature at the junction of two waveguides of opposite curvature, as in an S-shaped segment, leads to additional mode-coupling losses. In our simulations we fixed the waveguide height to 123 nm and, by means of a finite-difference frequency-domain numerical code (COMSOL), we calculated the total losses of a small sequence of S-shaped segments as a function of the curvature radius R. A schematic of the simulated snake-shaped waveguide is shown in Fig. 2(g). As a first result, we found that the bending loss coefficient decays exponentially with the curvature radius, so that it turns out to be negligible, both at FF and SH, for curvature radius $R > 10$ μm. Hence, the main contribution

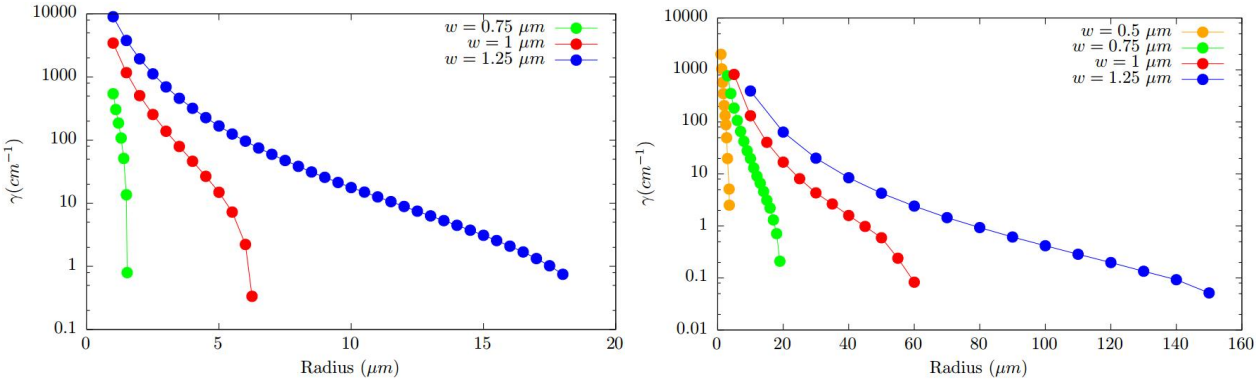

Figure 2. Loss coefficient γ as a function of the waveguide radius R, for different values of the waveguide width w at the FF (left) and SH (right).

to internal losses comes from mode overlap mismatch. Figure 2 shows the loss coefficient, for different waveguide widths w, as a function of the waveguide radius for the FF (left) and SH (right), respectively. As we can see, for structures with a curvature radius $R > 20$ μm and $w = 0.75$ μm, we found total losses lower than 1 cm^{-1} at both FF and SH. Moreover, mode-mismatch losses can be further minimized by the introduction of a lateral offset between the two opposite curvature sections.[18]

As the radius of curvature is directly determined by the coherence length of the nonlinear process to be phase matched, we also studied the tailoring of the modal dispersion by an appropriate choice of the waveguide geometry, aiming to increase the coherence length, hence reducing the bending losses. More in details, the coherence length for SHG is defined as:

$$L_c = \frac{\lambda}{4} \frac{1}{n_2^{\text{eff}} - n_1^{\text{eff}}}, \tag{1}$$

where n_1^{eff} and n_2^{eff} are the effective refractive indexes at the FF and SH, respectively. By means of numerical simulations we verified that, for an $Al_{0.18}Ga_{0.82}As$ ridge waveguide, the coherence length can be increased up to a few millimeters by a proper geometrical reshaping of the medium dispersion, through the waveguide width, as shown in Fig. 3.

Finally, to make a comparison with other phase matching techniques, we calculated the theoretical normalized SHG conversion efficiency for the previous structures as $\eta_{\text{norm}} = P_{\text{SH}}/(P_{\text{p}}L)^2 \simeq 200$ W^{-1}cm^{-2}, where P_{p}, P_{SH} represent the power at the FF and SH, respectively, and L is length of the structure under study. This efficiency is comparable to the one achievable in artificially birefringent AlGaAs waveguides,[19] and almost two orders of magnitude higher than what is available with GaAs/AlGaAs waveguides operated with modal phase-matching.[20]

3. INTERNALLY PUMPED OPO

Frequency comb generation has been experimentally demonstrated through continuously pumped cavity-enhanced SHG, where multiple cascaded $\chi^{(2)}$ nonlinear processes enable the onset of broadband comb emission, both around the FF pump frequency and its SH.[3] In detail, the SH power generated within the material can exceed the threshold for an internally-pumped optical parametric oscillator (IP-OPO), which in turn triggers a cascade of secondary three-wave processes, eventually leading to frequency combs formation. As the onset of IP-OPO is the main signature of the subsequent frequency comb generation, we investigated the power threshold for IP-OPO in $Al_{0.18}Ga_{0.82}As$ suspended-waveguide resonators with directional quasi-phase matched SHG. SH and sum-frequency generation processes, representing the leading nonlinear loss term, vanish at the minimum theoretical OPO threshold. Also, the other nonlinear processes starting just above the OPO threshold can be neglected to the first order in the parametric fields amplitude.[21] Therefore, we restrain our analysis to the nonlinear interactions involving only SHG and internally pumped OPO,[22] which are described by the following

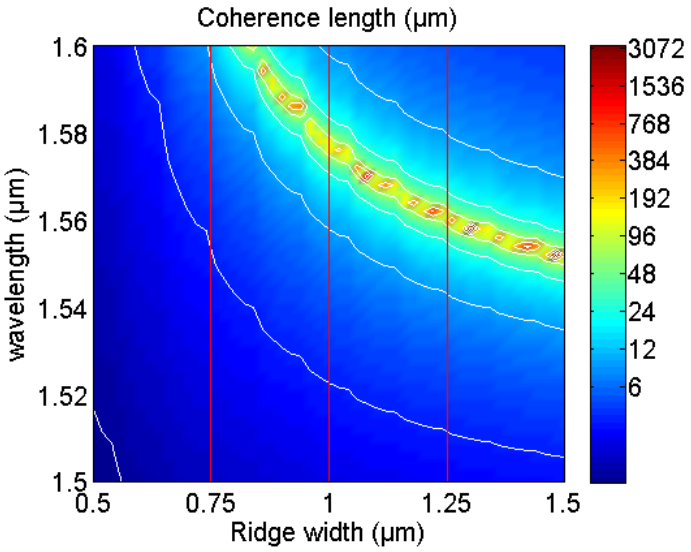

Figure 3. Coherence length as a function of the waveguide ridge width w and the fundamental wavelength.

coupled-mode equations for the fundamental, A_1, second-harmonic, A_2, and parametric (signal and idler) electric field amplitudes, $A_{\rm S}$ and $A_{\rm i}$, respectively,

$$\frac{dA_1}{d\zeta} = -\frac{\gamma_1}{2}A_1 - i\kappa\,\sigma(\zeta)\,A_1^* A_2\,e^{-i\Delta k\,\zeta} \tag{2}$$

$$\frac{dA_2}{d\zeta} = -\frac{\gamma_2}{2}A_2 - i\kappa\,\sigma(\zeta)\left(\frac{1}{2}\,A_1^2\,e^{i\Delta k\,\zeta} + A_{\rm S}A_{\rm i}\,e^{i\Delta K\,\zeta}\right) \tag{3}$$

$$\frac{dA_{\rm s,i}}{d\zeta} = -\frac{\gamma_{\rm s,i}}{2}A_{\rm s,i} - i\kappa\,\sigma(\zeta)\,A_{\rm i,s}^* A_2\,e^{-i\Delta K\,\zeta}\,. \tag{4}$$

where the γ's represent the internal power loss coefficients, $\Delta k = k_2 - 2k_1$ and $\Delta K = k_2 - k_{\rm S} - k_{\rm i}$ are the mismatch wave vectors for SHG and OPO, respectively, with $k_j = 2\pi n_j/\lambda_j$ and $j \in \{1, 2, {\rm s}, {\rm i}\}$; the nonlinear coupling constant, $\kappa = (d_{14}/c)\sqrt{2\omega_1^3/n_1^2\,n_2}$, is assumed to be the same for all processes, where $d_{14} = 100$ pm/V is the quadratic nonlinear coefficient of AlGaAs, c the speed of light, $\omega_1 = 2\pi c/\lambda_1$ the angular frequency of the pump, and n_j the refractive index at wavelength λ_j. Field amplitudes are normalized so that $|A|^2$ is a photon number.

4. SIMULATIONS RESULTS

In order to calculate the IP-OPO power threshold, we numerically solved Eqs. (2-4) for the field amplitudes, by iteratively propagating over a round trip, $\zeta \in [0, L]$, until a steady-state is reached and according to the boundary conditions:

$$A_j^{(m+1)}(0) = (1-\theta_j)^{1/2} A_j^{(m)}(L)\,e^{-i\Delta_j} + \delta_{j1}\theta_j^{1/2} A_{1,in},$$

where θ_j is the power transmission coefficient of the incoupling port for the jth field, Δ_j is the frequency detuning between the jth field and the nearest cavity resonance, δ_{j1} the Kroneckers delta, and $A_{1,in}$ the constant input field amplitude. The power threshold for the IP-OPO corresponds to the pump power value that intercepts the x-axis in the linear fit of intracavity signal power vs. pump power plot.

Considering resonant structures composed of $2N$ and $2M$ S-segments and 4 corner A-segments, with length $L = 2(N + M + 2)L_c$, (see Fig. 1(d) for $M = 2$ and $N = 2$), we analyze the IP-OPO pump power threshold as a function of the resonator length, assuming spectrally dependent coupling coefficients, θ_p and θ_h, for FF and SH, respectively. We set the value of the S-segment curvature radius to $R = 20$ μm, i.e., $L_c = \pi R \simeq 63$ μm, for which we know the total losses α can be kept below 1 dB/cm, once we fixed $w = 0.75$ μm. Note that the coefficient α,

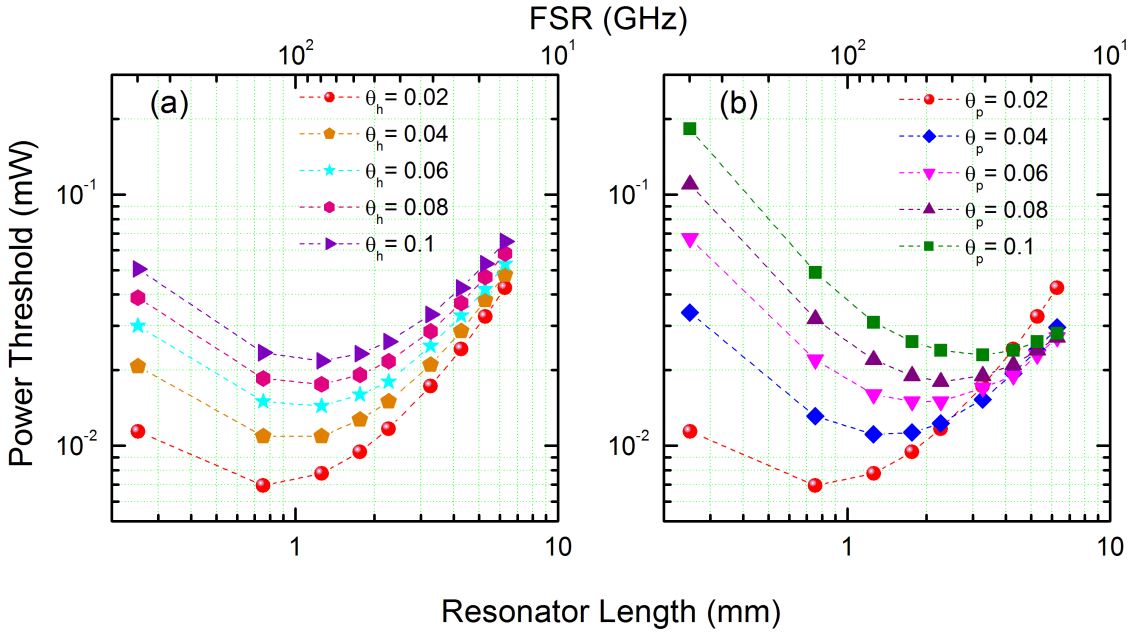

Figure 4. Internally pumped OPO power threshold vs. resonator length, for internal losses of 1 dB/cm and different values of power transmission coefficients: (a) $\theta_p = 0.02$ and $0.02 \leq \theta_h \leq 0.1$, (b) $\theta_h = 0.02$ and $0.02 \leq \theta_p \leq 0.1$. The corresponding free spectral range scale is reported on the top axis. Dashed lines are given as guides to the eye.

given in dB per-unit-length, is related to the coefficient γ (inverse of the unit length) as $\gamma_j \simeq 0.23\,\alpha_j$. We assume FF and SH to be perfectly resonant ($\Delta_1 = \Delta_2 = 0$). Also, because of the nearly degenerate IP-OPO operation, we may safely neglect the effect of cavity dispersion; thus, we assume $\Delta K = \Delta k = \pi/L_c$, and zero detuning for the parametric fields as well ($\Delta_s = \Delta_i = 0$). With these conditions, we have estimated the IP-OPO power threshold for different values of the power transmission coefficients θ_j and internal losses of 1 dB/cm.

Figure 4 shows the calculated IP-OPO pump power threshold as a function of the resonator length (FSR ranging from 15 to 380 GHz), for internal losses of 1 dB/cm and different values of transmission coefficients. For the case $\theta_p = \theta_h = 0.02$, we get the lowest pump power threshold, around 7 μW, for a resonator length of 750 μm. For $\theta_p = 0.02$ and different values of the SH coupling coefficient, the IP-OPO power threshold increases with θ_h as expected, remaining however below 100 μW. Whereas, for each θ_h, the minimum threshold occurs for resonator lengths around 1 mm, with a weak dependence on θ_h. Interestingly, the simulations for a fixed harmonic coupling coefficient $\theta_h = 0.02$ show that, for progressively increasing fundamental coupling coefficients θ_p, the minimum IP-OPO power threshold corresponds to longer resonator lengths. Moreover, whilst for lower resonator lenghts the threshold increases with θ_p, for the highest studied resonator lengths the threshold sightly decreases as θ_p increases (see Fig. 4(b)).

More generally, it is possible to optimize the OPO threshold for a wide range of round trip lengths, from 250 μm up to several mm, by suitably designing the in/out coupling port parameters. The optimization of the OPO threshold guarantees high conversion efficiencies in the cascade of multiple nonlinear generations that lead to comb formation, with a minimum expected teeth spacing equal to the resonator free spectral range, $\mathrm{FSR} = c/n_1 L$.

We also calculated the quality factor Q of the proposed structures at the FF frequency. Figure 5 shows the Q factor as a function of the resonator length for different values of the total loss coefficient α (0.5, 1, and 2 dB/cm). We observe in Fig. 5 that in the correspondence of the lowest loss coefficient (0.5 dB/cm) the Q factor strongly depends on the cavity length, while for losses of 2 dB/cm and resonators longer than 3 mm, the

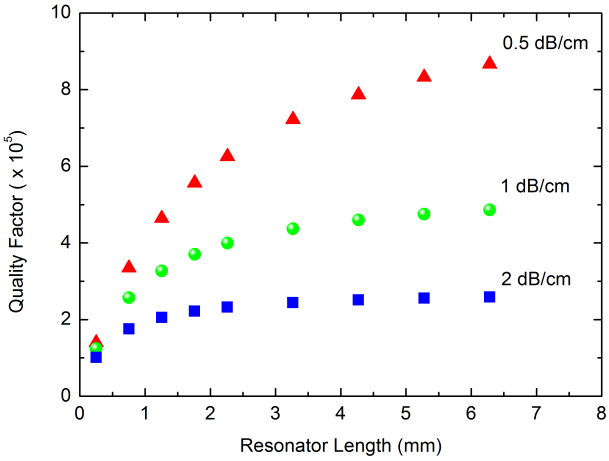

Figure 5. Q factor at the FF frequency for an $Al_{0.18}Ga_{0.82}As$ structure as a function of the resonator length for three values of total losses α: 0.5 dB/cm (triangles), 1 dB/cm (circles) and 2 dB/cm (squares).

Q factor value essentially remains constant around 2×10^5. Furthermore, even for the highest values of the loss coefficient, 2 dB/cm, a high-quality-factor ($Q > 10^5$) microresonator can still be obtained.

Finally, the spectral dynamics of frequency comb generation can be numerically studied by solving the infinite-dimensional map for the field envelopes centered around the FF and SH,[4] which can suitably describe the full comb dynamics, not being restrained to only four modes as Eqs. (2-4). As an example, Fig. 6 reports the power spectral densities of multiple frequency components around the FF and SH, obtained for resonant structures with a length of 1.76 mm, $\alpha = 1\,\mathrm{dB/cm}$, $\theta_h = 0.02$ and $\theta_p = 0.04$, respectively. Here we can distinguish two different scenarios of comb formation, depending on the pump power. For a pump power of 50 μW, around five times the 11-μW threshold for the IP-OPO, a 20 nm (10 nm) wide comb is established around the FF (SH), with a line spacing of one FSR (54 GHz) (see Figs. 6(a) and (b)). For a pump power of 500 μW, the spectral features change and a set of multimode spaced (13 FSR) subcombs appear, with individual line spacing of one FSR, Figs. 6(c) and (d).

5. CONCLUSIONS

We proposed a novel design for AlGaAs quadratic nonlinear waveguide resonators to realize efficient frequency comb generation, by exploiting the DQPM SHG mechanism. The proposed resonator geometry consists of a proper sequence of arc- and S-shaped segments in a closed loop that exhibits internal losses lower than 1 dB/cm, for curvature radius of 20 μm, corresponding to a Q as high as 10^5. By numerical simulations, we have shown that OFC generation is possible with pump threshold powers of a few μW, teeth separations in the range of 10-1000 GHz, which are suitable for different applications in the fields of spectroscopy and telecom, and with spectra spanning more than 5 THz. Such a comb synthesizer, combining small-size photonic circuits and the strong quadratic nonlinearity of AlGaAs, can be inherently more efficient than Kerr combs, and it is capable of direct multi-octave emission, having significantly lower power threshold. A direct, though partial, comparison can be made with recent, mW-level, third-order nonlinear comb generation in high-quality AlGaAs microresonators.[23] Because of the wide transparency window of AlGaAs materials, the quadratic frequency combs described here can be potentially extended into the mid-infrared region for applications in frequency metrology and spectroscopy.

ACKNOWLEDGMENTS

M.D.R. acknowledges support from Consiglio Nazionale delle Ricerche through the Short-Term Mobility Program 2016.

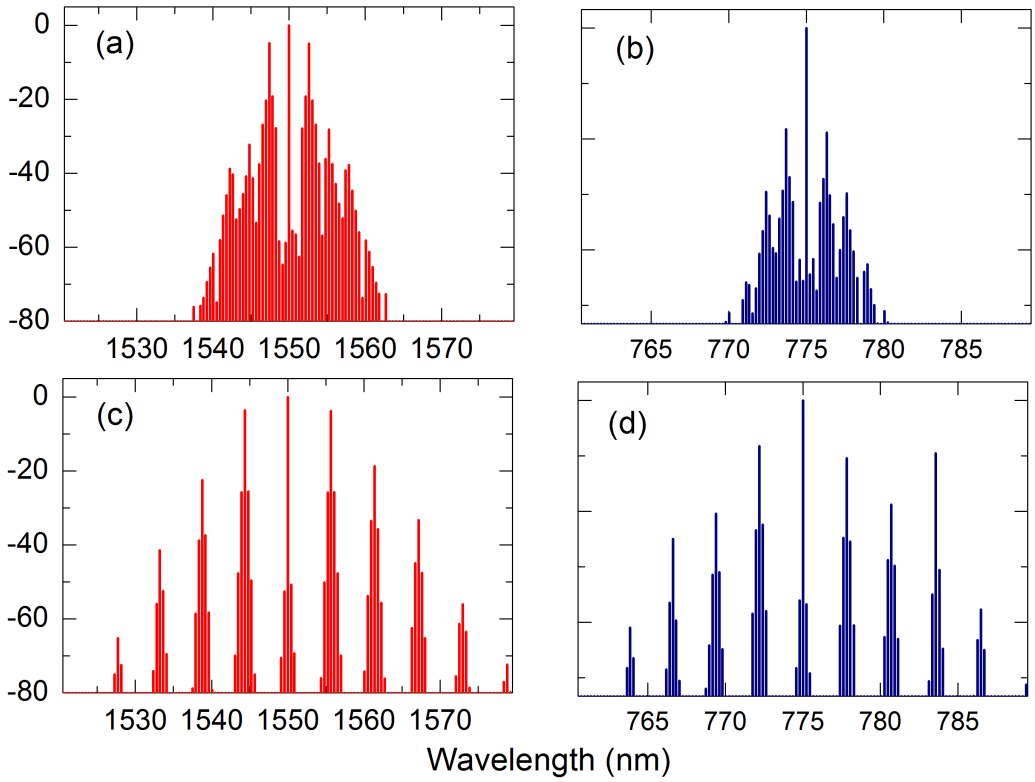

Figure 6. Numerically simulated frequency combs for resonant structures with $L = 1.76$ mm, $\alpha = 1$ dB/cm, $\theta_h = 0.02$ and $\theta_p = 0.04$. (a) and (c) show the FF spectra for 50 μW and 500 μW of pump power, respectively. The corresponding SH spectra are shown in (b) and (d).

REFERENCES

[1] Del'Haye, P., Schliesser, A., Arcizet, O., Wilken, T., Holzwarth, R., and Kippenberg, T. J., "Optical frequency comb generation from a monolithic microresonator," *Nature* **450**, 1214–1217 (2007).

[2] Ulvila, V., Phillips, C. R., Halonen, L. L., and Vainio, M., "Frequency comb generation by a continuous-wave-pumped optical parametric oscillator based on cascading quadratic nonlinearities," *Opt. Lett.* **38**, 4281 (2013).

[3] Ricciardi, I., Mosca, S., Parisi, M., Maddaloni, P., Santamaria, L., De Natale, P., and De Rosa, M., "Frequency comb generation in quadratic nonlinear media," *Phys. Rev. A* **91**, 063839–10 (2015).

[4] Leo, F., Hansson, T., Ricciardi, I., De Rosa, M., Coen, S., Wabnitz, S., and Erkintalo, M., "Walk-Off-Induced Modulation Instability, Temporal Pattern Formation, and Frequency Comb Generation in Cavity-Enhanced Second-Harmonic Generation," *Phys. Rev. Lett.* **116**, 033901–6 (2016).

[5] Leo, F., Hansson, T., Ricciardi, I., De Rosa, M., Coen, S., Wabnitz, S., and Erkintalo, M., "Frequency-comb formation in doubly resonant second-harmonic generation," *Phys. Rev. A* **93**, 043831 (2016).

[6] Hansson, T., Leo, F., Erkintalo, M., Anthony, J., Coen, S., Ricciardi, I., De Rosa, M., and Wabnitz, S., "Single envelope equation modeling of multi-octave comb arrays in microresonators with quadratic and cubic nonlinearities," *J. Opt. Soc. Am. B* **33**, 1207–1215 (2016).

[7] Helmy, A. S., Abolghasem, P., Stewart Aitchison, J., Bijlani, B. J., Han, J., Holmes, B. M., Hutchings, D. C., Younis, U., and Wagner, S. J., "Recent advances in phase matching of second-order nonlinearities in monolithic semiconductor waveguides," *Laser & Photon. Rev.* **5**, 272–286 (2010).

[8] Caspani, L., Duchesne, D., Dolgaleva, K., Wagner, S. J., Ferrera, M., Razzari, L., Pasquazi, A., Peccianti, M., Moss, D. J., Aitchison, J. S., and Morandotti, R., "Optical frequency conversion in integrated devices," *J. Opt. Soc. Am. B* **28**, A67–A82 (2011).

[9] Savanier, M., Ozanam, C., Ghiglieno, F., Lafosse, X., Lemaître, A., Favero, I., Ducci, S., Leo, G., and Lanco, L. in [*Optoelectronics - Advanced Materials and Devices*], Pyshkin, S., ed., 1–32, InTech (2013).

[10] Dumeige, Y. and Féron, P., "Whispering-gallery-mode analysis of phase-matched doubly resonant second-harmonic generation," *Phys. Rev. A* **74**, 063804–7 (2006).

[11] Yang, Z., Chak, P., Bristow, A. D., van Driel, H. M., Iyer, R., Aitchison, J. S., Smirl, A. L., and Sipe, J. E., "Enhanced second-harmonic generation in AlGaAs microring resonators.," *Opt. Lett.* **32**, 826–828 (2007).

[12] Kuo, P. S., Fang, W., and Solomon, G. S., "$\bar{4}$-quasi-phase-matched interactions in GaAs microdisk cavities.," *Opt. Lett.* **34**, 3580–3582 (2009).

[13] Kuo, P. S. and Solomon, G. S., "On- and off-resonance second-harmonic generation in GaAs microdisks," *Opt. Express* **19**, 16898–16918 (2011).

[14] Horn, R. T. and Weihs, G., "Directional quasi-phase matching in curved waveguides," arXiv 1008.2190 (2010).

[15] Kuo, P. S., Bravo-Abad, J., and Solomon, G. S., "Second-harmonic generation using $\bar{4}$-quasi-phasematching in a GaAs whispering-gallery-mode microcavity.," *Nat. Commun.* **5**, 3109 (2014).

[16] Mariani, S., Andronico, A., Lemaître, A., Favero, I., Ducci, S., and Leo, G., "Second-harmonic generation in AlGaAs microdisks in the telecom range," *Opt. Lett.* **39**, 3062–3065 (2014).

[17] Baker, C., Belacel, C., Andronico, A., Senellart, P., Lemaître, A., Galopin, E., Ducci, S., Leo, G., and Favero, I., "Critical optical coupling between a GaAs disk and a nanowaveguide suspended on the chip," *Appl. Phys. Lett.* **99**, 151117 (2011).

[18] Pennings, E. C. M., Manhoudt, G. H., and Smit, M. K., "Low-loss bends in planar optical ridge waveguides," *Electron. Lett.* **24**, 998–999 (1988).

[19] Scaccabarozzi, L., Fejer, M. M., Huo, Y., Fan, S., Yu, X., and Harris, J. S., "Enhanced second-harmonic generation in AlGaAs/AlxOy tightly confining waveguides and resonant cavities," *Opt. Lett.* **31**, 3626–3628 (2006).

[20] Ducci, S., Lanco, L., Berger, V., De Rossi, A., Ortiz, V., and Calligaro, M., "Continuous-wave second-harmonic generation in modal phase matched semiconductor waveguides," *Appl. Phys. Lett.* **84**, 2974–2976 (2004).

[21] Mosca, S., Ricciardi, I., Parisi, M., Maddaloni, P., Santamaria, L., De Natale, P., and De Rosa, M., "Direct generation of optical frequency combs in $\chi^{(2)}$ nonlinear cavities," *Nanophotonics* **5**, 316–331 (2016).

[22] Schiller, S., Bruckmeier, R., and White, A. G., "Classical and quantum properties of the subharmonic-pumped parametric oscillator," *Opt. Commun.* **138**, 158–171 (1997).

[23] Pu, M., Ottaviano, L., Semenova, E., and Yvind, K., "Efficient frequency comb generation in AlGaAs-on-insulator," *Optica* **3**, 823–826 (2016).